Conducting Polymer Diffraction Gratings on Gold Surfaces Created by Microcontact Printing and Electropolymerization at Submicron Length Scales

F. Saneeha Marikkar,[†] Chet Carter,[‡] Kathy Kieltyka, Joseph W. F. Robertson,[§] Cathie Williamson, Adam Simmonds, Rebecca Zangmeister,[§] Torsten Fritz,[⊥] and Neal R. Armstrong*

Department of Chemistry, University of Arizona, Tucson, Arizona 85721

Received May 11, 2007. In Final Form: July 11, 2007

Conducting polymer diffraction gratings on Au substrates have been created using microcontact printing of C_{18}-alkanethiols, followed by electropolymerization of either poly(aniline) (PANI) or poly(3,4-ethylenedioxythiophene) (PEDOT). Soft-polymer replicas of simple diffraction grating masters (1200 lines/mm) were used to define the alkanethiol template for polymer growth. Growth of PANI and PEDOT diffraction gratings was followed in real time, through in situ tapping-mode atomic force microscopy, and by monitoring diffraction efficiency (DE) as a function of grating depth. DE increased as grating depth increased, up to a limiting efficiency (13−26%, with white light illumination), defined by the combined optical properties of the grating and the Au substrate, and ultimately limited by the loss of resolution due to coalescence of the polymer films. Grating efficiency is strongly dependent upon the grating depth and the refractive index contrast between the grating material and the surrounding solutions. Both PEDOT and PANI gratings show refractive index changes as a function of applied potential, consistent with changes in refractive index brought about by the doping/dedoping of the conducting polymer. The DE of PANI gratings are strongly dependent on the pH of the superstrate solution; the maximum sensitivity ($\Delta DE/\Delta pH$) is achieved with PANI gratings held at +0.4 V versus Ag/AgCl, where the redox chemistry is dominated by the acid−base equilibrium between the protonated (emeraldine salt) and deprotonated (emeraldine base) forms of PANI. Simulations of DE were conducted for various combinations of conducting polymer refractive index and grating depth, to compute sensitivity parameters, which are maximized when the grating depth is ca. 50% of its maximum obtainable depth.

Introduction

Conducting polymer (CP) thin films are increasingly used as sensor transducer layers, especially if both their electrochemical and optical properties can be interrogated simultaneously.[1−18] Both the real component (n) and imaginary component (k) of the refractive index of these materials change dramatically as they are cycled through their oxidized and reduced forms.[1−4,19−23] Binding of certain analyte species can alter the potentials required to oxidize and reduce the polymer, or they can be oxidized (reduced) electrocatalytically, so that either amperometric or potentiometric detection can be coupled with optical interrogation methods to extend both the sensitivity and selectivity of analyte detection.[3,4,17−19] Schanze and co-workers[1] and Hupp and co-workers[2] recently showed that the patterning of CP films on the micron scale can be used to form chemically and electrochemically responsive diffraction gratings, which may have significant analytical utility. Hammond et al.[24,25] and Yang et al.[26] created polymer micropatterns by exploiting wettability differences on polymer substrates. Stevenson and co-workers recently created regular spaced submicron voids using the negative pattern of a microsphere layer.[9] Diffraction gratings have also been formed from other chemically responsive materials, including antibodies, enzymes, nanowires, and nanoparticles, showing a high sensitivity of changes in diffraction efficiency (DE) versus changes in

* Corresponding author. E-mail: nra@u.arizona.edu.
[†] Current address: Huntsman Chemical, Inc., Longview, Texas.
[‡] Current address: Micron Industries, Boise, Idaho.
[§] Current address: National Institute for Standards and Technology, Gaithersburg, Maryland.
[⊥] Institute für Angewandte Photophysik, Technische Universität Dresden, Dresden, Germany.

(1) Schanze, K. S.; Bergstedt, T. S.; Hauser, B. T.; Cavalaheiro, C. S. P. *Langmuir* **2000**, *16*, 795−810.
(2) Massari, A. M.; Stevenson, K. J.; Hupp, J. T. *J. Electroanal. Chem.* **2001**, *500*, 185−191.
(3) Tian, S. J.; Armstrong, N. R.; Knoll, W. *Langmuir* **2005**, *21*, 4656−4660.
(4) Tian, S. J.; Baba, A.; Liu, J. Y.; Wang, Z. H.; Knoll, W.; Park, M. K.; Advincula, R. *Adv. Funct. Mater.* **2003**, *13*, 473−479.
(5) Baba, A.; Lubben, J.; Tamada, K.; Knoll, W. *Langmuir* **2003**, *19*, 9058−9064.
(6) Wang, Y. J.; Knoll, W. *Anal. Chim. Acta* **2006**, *558*, 150−157.
(7) Baba, A.; Knoll, W. *J. Phys. Chem. B* **2003**, *107*, 7733−7738.
(8) Xia, C. J.; Advincula, R. C.; Baba, A.; Knoll, W. *Langmuir* **2002**, *18*, 3555−3560.
(9) Maldonado, S.; Smith, T. J.; Williams, R. D.; Morin, S.; Barton, E.; Stevenson, K. J. *Langmuir* **2006**, *22*, 2884−2891.
(10) Genies, E. M.; Lapkowski, M. *J. Electroanal. Chem.* **1987**, *220*, 67−82.
(11) Schanze, K. S.; Bergstedt, T. S.; Hauser, B. T. *Adv. Mater.* **1996**, *8*, 531−534.
(12) Karyakin, A. A.; Bobrova, O. A.; Luckachova, L. V.; Karyakina, E. E. *Sens. Actuators, B* **1996**, *33*, 34−38.
(13) Raitman, O. A.; Katz, E.; Buckmann, A. F.; Willner, I. *J. Am. Chem. Soc.* **2002**, *124*, 6487−6496.
(14) Lindfors, T.; Ivaska, A. *J. Electroanal. Chem.* **2002**, *535*, 65−74.
(15) Lindfors, T.; Ivaska, A. *J. Electroanal. Chem.* **2002**, *531*, 43−52.
(16) Lindfors, T.; Kvarnstrom, C.; Ivaska, A. *J. Electroanal. Chem.* **2002**, *518*, 131−138.
(17) McBee, T. W.; Wang, L. Y.; Ge, C. H.; Beam, B. M.; Moore, A. L.; Gust, D.; Moore, T. A.; Armstrong, N. R.; Saavedra, S. S. *J. Am. Chem. Soc.* **2006**, *128*, 2184−2185.
(18) Ge, C.; Armstrong, N. R.; Saavedra, S. S. *Anal. Chem.* **2007**, *79*, 1401−1410.
(19) Kim, D. R.; Cha, W.; Paik, W. K. *Synth. Met.* **1997**, *84*, 759−760.
(20) Redondo, A.; Ticianelli, E. A.; Gottesfeld, S. *Mol. Cryst. Liq. Cryst.* **1988**, *160*, 185−203.
(21) Gottesfeld, S. *J. Electroanal. Chem.* **1989**, *15*, 143−265.
(22) Redondo, A.; Ticianelli, E. A.; Gottesfeld, S. *Synth. Met.* **1989**, *29*, E265−E270.
(23) Pettersson, L. A. A.; Carlsson, F.; Inganas, O.; Arwin, H. *Thin Solid Films* **1998**, *313*, 356−361.
(24) Hammond, P. T.; Whitesides, G. M. *Macromolecules* **1995**, *28*, 7569−7571.
(25) Jiang, X. P.; Hammond, P. T. *Langmuir* **2000**, *16*, 8501−8509.
(26) Yang, P.; Xie, J. Y.; Yang, W. T. *Macromol. Rapid Commun.* **2006**, *27*, 418−423.

10.1021/la701369h CCC: $37.00
Published on Web 08/28/2007 PAGE EST: 7.6

solution analyte concentration.[27−32] The pH sensing capabilities of highly absorbing CP films and the potential dependent electrochromic behavior of CP films in periodic geometries appear to meet or exceed the sensitivity of conventional thin-film-based optical sensors.[3,17,18] Knoll and co-workers have recently coupled the formation of chemically responsive diffraction gratings to conventional surface plasmon resonance (SPR) characterization of CP films on gold substrates.[3] These SPR-enhanced CP diffraction gratings are extremely sensitive to the redox state of the CP film and can be extended to the characterization of the adsorption/oxidation of analytes such as β-nicotinamide adenine dinucleotide (NADH).[4,33]

We show here that a simple combination of submicron-scale microcontact printing of alkanethiols on gold (using a soft-polymer (poly(dimethylsiloxane) (PDMS) stamp created from a blazed gold-coated master grating), followed by electrochemical growth of either poly(aniline) (PANI) or poly(3,4-ethylenedioxythiophene) (PEDOT) produces diffraction gratings that function throughout the visible wavelength region with DEs in excess of 13%, nearly twice that observed for the gold-coated master gratings used to create the soft polymer stamp. Grating formation is followed both by in situ atomic force microscopy (AFM) and optically, in real time, and is shown to qualitatively follow the change in DE versus grating depth, the refractive index of the grating material, and changes in n and k, during chemical changes to the grating material, predicted from solutions of Maxwell's equations for conventional grating systems. DEs are controlled by the duration of electropolymerization (which controls the grating depth), by the extent of electrochemical doping/dedoping of these films, and by changes in electrolyte composition (e.g., for PANI gratings, changes in pH). Changes in DE are most strongly dependent upon changes in the refractive index of the grating elements, providing information that is complementary to that obtained from either ellipsometric[19,34−38] or SPR techniques,[5,6,39−41] on an appealingly simple platform.

Experimental

The PDMS stamp was produced by conventional means.[42,43] A gold-coated "master" grating (1200 lines/mm; grating period = 833 nm, blaze angle = 36°, grating depth = ca. 100 nm, grating area = ca. 1 cm^2; Edmund Optics) was used to make the PDMS mold. This stamp was constructed by placing the grating master in a level container where a 10:1 (w/w) mixture of SYLGARD silicone elastomer 184 and SYLGARD 184 curing agent (DOW Corning Corporation) was allowed to envelope the master. This assembly was left to degas at room temperature for 1−2 h until the elastomer block was free of visible air bubbles, and was then cured for 8 h at ca. 90 °C. The PDMS block was then gently peeled back from the grating master and cut to size with a razor. A scanning electron micrograph shows the features on such a stamp (Figure 1), showing that the molding process produces features with a large aspect ratio, which are relatively deep (up to 100 nm grating depth).

Electrochemically blocked regions on the Au surface were produced by conventional microcontact printing using these patterned PDMS stamps. An octadecanethiol (C_{18}−SH)/ethanol (10^{-4} M) ink was placed on the stamp for 1 min, the excess was rinsed away, and the stamp was dried in a stream of nitrogen. A simple clamp apparatus was constructed to hold the PDMS stamp, providing for constant vertical alignment with the surface to be stamped, to ensure normal, even stamping with constant pressure across the entire stamped surface. For submicron features this is a critical modification to the microcontact printing process. The inked stamp was brought into contact with the clean Au thin film with a force of ca. 1−2 kg/cm^2, for 1 min, then was quickly separated from the gold surface, which was rinsed and dried.

Most of the Au electrodes used were cleaned 100 nm Au vapor-deposited films on a Cr adhesion layer on conventional microscope slides (root-mean-square (rms) roughness ca. 1−3 nm) (Evaporated Metal Films, Ithaca, NY). These electrodes were cleaned by (a) rinsing in a piranha solution for 1 min, followed by rinsing in triply distilled water, or (b) by electrochemically cleaning the Au electrodes by cycling their potential from 0.0 to +1.5 V, versus Ag/AgCl, in the supporting electrolyte solution (see below), forming and reducing the gold surface oxide. A few gratings were grown on ultrasmooth Au on glass produced by a "template stripping" process recently described by Knoll and co-workers,[44] which consists of evaporating ca. 100 nm Au films on Si(100) wafers, followed by gluing a piece of glass to the top side of the Au film, and then cleaving the cured slide to expose a clean and extremely smooth (rms roughness less than 1 nm) Au surface. The rinsed/dried Au electrodes were immediately stamped with the C_{18}-thiol solution in a laminar flood hood environment, which kept dust particles from adsorbing to the electrode surface.

A small-volume variant of normal spectroelectrochemical cells was used to grow and characterize CP grating structures.[45,46] Grating features with excellent uniformity, over electrode areas of ca. 1 cm^2, were achieved by using a semitransparent indium tin oxide (ITO)/glass electrode as the counter electrode, placed directly opposite the gold working electrode, with a separation between the grating electrode and the counter electrode of less than ca. 0.3 cm. This small volume cell was configured to allow several different solutions to be brought into contact with the grating, without the need to change the position of the cell. The use of a semi-transparent counter electrode allowed "frontside" optical characterization of the DE during grating formation, and during/after exposure to different electrolyte solutions as described below. The uniform current flow across ca. l cm^2 electrode areas was found to be critical to obtain high-quality large-area CP gratings. The DE was generally measured using 633 nm excitation (5 mW He−Ne), with s- or p-polarization, incident at 45° or 90° to the surface normal, monitoring the first order ($m = 1$ or $m = -1$) diffraction spot. Occasional measurements were made with a green-emitting He−Ne laser (534 nm).

CP/Au gratings were generally grown by potential step techniques. PEDOT gratings were grown from methanol/water, 10% v/v MeOH, 0.1 M $LiClO_4$, 0.01 M EDOT monomer or acetonitrile, 0.1 M $LiClO_4$, 0.01 M EDOT monomer solutions at an applied potential of +1.0 V versus Ag/AgCl. PANI gratings were grown from 0.5 M H_2SO_4,

(27) Bailey, R. C.; Nam, J. M.; Mirkin, C. A.; Hupp, J. T. *J. Am. Chem. Soc.* **2003**, *125*, 13541−13547.
(28) St. John, P. M.; Davis, R.; Cady, N.; Czajka, J.; Batt, C. A.; Craighead, H. G. *Anal. Chem.* **1998**, *70*, 1108−1111.
(29) Loo, R. W.; Tam, P. L.; Goh, J. B.; Goh, M. C. *Anal. Biochem.* **2005**, *337*, 338−342.
(30) Schider, G.; Krenn, J. R.; Gotschy, W.; Lamprecht, B.; Ditlbacher, H.; Leitner, A.; Aussenegg, F. R. *J. Appl. Phys.* **2001**, *90*, 3825−3830.
(31) Pan, Z. W.; Mahurin, S. M.; Dai, S.; Lowndes, D. H. *Nano Lett.* **2005**, *5*, 723−727.
(32) Adleman, J. R.; Eggert, H. A.; Buse, K.; Psaltis, D. *Opt. Lett.* **2006**, *31*, 447−449.
(33) Bartlett, P. N.; Simon, E. *Phys. Chem. Chem. Phys.* **2000**, *2*, 2599−2606.
(34) Chao, F.; Costa, M.; Museux, E.; Levart, E.; Abrantes, L. M. *Soviet Electrochem.* **1993**, *29*, 73−81.
(35) Abrantes, L. M.; Correia, J. P. *Electrochim. Acta* **1999**, *44*, 1901−1910.
(36) Topart, P.; Hourquebie, P. *Thin Solid Films* **1999**, *352*, 243−248.
(37) Xie, D.; Jiang, Y. D.; Pan, W.; Li, D.; Wu, Z. M.; Li, Y. R. *Sens. Actuators, B* **2002**, *81*, 158−164.
(38) Abrantes, L. M.; Correia, J. P.; Savic, M.; Jin, G. *Electrochim. Acta* **2001**, *46*, 3181−3187.
(39) Raty, J.; Peiponen, K. E.; Jaaskelainen, A.; Makinen, M. O. A. *Appl. Spectrosc.* **2002**, *56*, 935−941.
(40) Kurihara, K.; Nakamura, K.; Hirayama, E.; Suzuki, K. *Anal. Chem.* **2002**, *74*, 6323−6333.
(41) Ekgasit, S.; Tangcharoenbumrungsuk, A.; Yu, F.; Baba, A.; Knoll, W. *Sens. Actuators, B* **2005**, *105*, 532−541.
(42) Zangmeister, R. A. P.; O'Brien, D. F.; Armstrong, N. R. *Adv. Funct. Mater.* **2002**, *12*, 179−186.
(43) Xia, Y. N.; Whitesides, G. M. *Angew. Chem., Int. Ed.* **1998**, *37*, 551−575.
(44) Naumann, R.; Schiller, S. M.; Giess, F.; Grohe, B.; Hartman, K. B.; Karcher, I.; Koper, I.; Lubben, J.; Vasilev, K.; Knoll, W. *Langmuir* **2003**, *19*, 5435−5443.
(45) Carter, C. Ph.D. Dissertation, University of Arizona, Tucson, AZ, 2006.
(46) Marikkar, F. S. Ph.D. Dissertation, University of Arizona, Tucson, AZ, 2006.

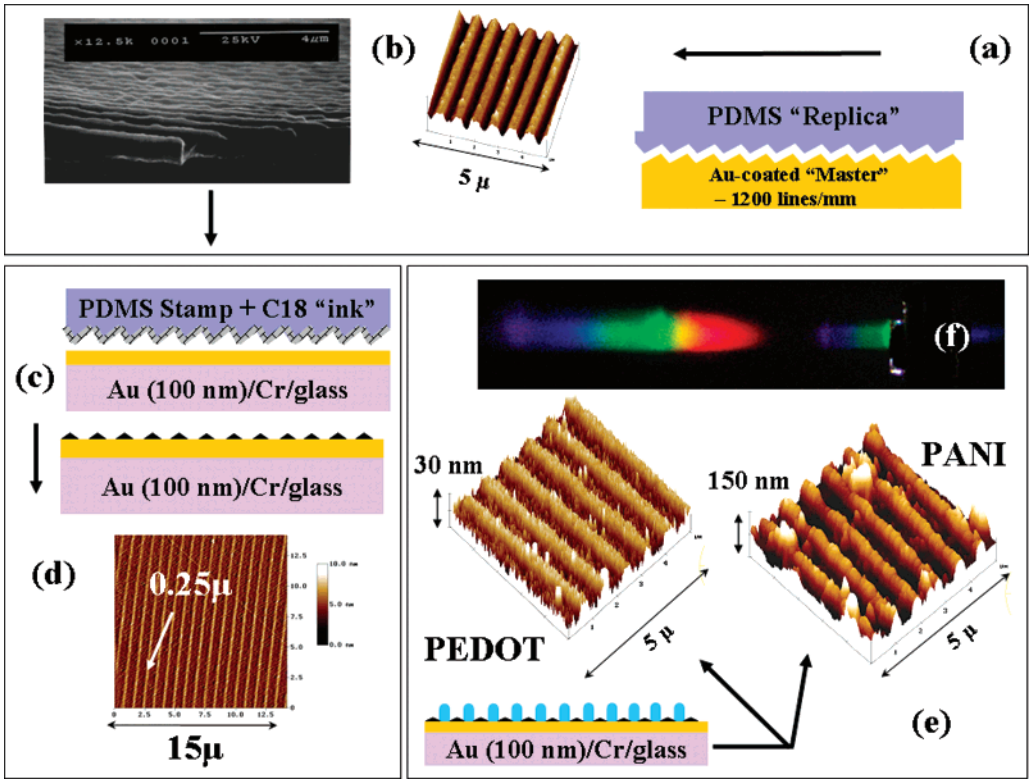

Figure 1. Schematic views of electrochemical growth of efficient diffraction gratings: (a) Formation of PDMS stamp from a grating "master"; (b) AFM and SEM images of resultant stamp, showing the roughness of the stamp features; (c) Stamping action (1−2 s) provides for integrity of stamped features, down to ca. 0.25 micron widths (shown by AFM image in panel d); (e) Electrochemical growth of both PEDOT and PANI patterned films. The AFM images shown correspond to a polymer film thickness typical for the most efficient gratings, and the bright spots represent nucleation sites where polymer growth is fastest, which eventually coalesce into continuous films, leading to loss of DE. (f) White light source image after diffraction by a PANI grating, showing both first-order diffraction (left side of image) and second-order diffraction (just half of that image is shown on the right side).

0.05 M aniline solutions at an applied potential of +0.7 V versus Ag/AgCl. To characterize the uniformity of grating growth on these surfaces, occasional experiments were conducted using cyclic voltammetry to control CP film growth, and simultaneous tapping-mode AFM on an electrochemically compatible scanning stage (Nanoscope III, Digital Instruments), in solutions of methanol/water, 10% v/v MeOH, 0.1M $LiClO_4$, and 0.01 M EDOT monomer. For each voltammetric cycle, the potential was swept past the onset for polymer (PEDOT) formation (ca. 0.9 V vs Ag/AgCl) and returned to its initial potential, and AFM images were obtained at the end of each cyclic voltammetric scan.

DE versus grating depth was simulated with Grating Solver V4.20 (Grating Solver Development Company, Allen, Texas), which features optimized algorithms that solve the vector Maxwell equations in the grating region, (see below for discussion). The CP grating is assumed to have a rectangular shape, with an aspect ratio of 1:1, coating a gold substrate with a complex index of refraction (at 633 nm) of $n = 1.6$ and $k = 0.14$.[47] The impact of the change in $n = 1.4-1.7$ relative to the refractive index of the supersaturated solution (n'), and the variations of $k = 0.1-1.0$ were also investigated.

Results and Discussion

Patterned Film Formation. Figure 1 shows a schematic view of the microcontact printing process, along with scanning electron microscopy (SEM) and AFM views of the PDMS stamp surface, and AFM images of thick PANI and PEDOT gratings (ca. 30−150 nm) just before they coalesced into continuous CP films (see below). Grating features are, in general, quite regular, but there are regions where polymer growth was accelerated, and it is these regions that eventually dominate film growth, causing the polymer film to become continuous and diffraction to cease. All of our sensing studies were therefore conducted with much thinner gratings (see below) to optimize changes in their optical properties with changes in applied potential and/or solution pH.

The SEM image of the PDMS stamp shows the roughness of the grating surface itself, transferred to the stamp, with asperities of up to 10−30 nm in height on the top of the PDMS features. Pressing the inked region onto the Au surface with sufficient force for brief periods of time and careful alignment of the stamp provide excellent transfer of the alkanethiol ink to the Au surface, with feature sizes down to 125 nm width, with excellent integrity. Even though the commercial grating used as a master was blazed, the final inked region on the Au surface and the subsequent CP gratings did not show evidence of this blazed condition. Recent work in our group suggests that this approach will allow gratings with excellent integrity to be formed up to 2400 lines/mm.[48]

The images in Figure 2 were obtained by cycling the potential of the patterned gold surface with simultaneous characterization between cycles by in situ tapping-mode AFM (methanol/water, 10% v/v MeOH, 0.1 M $LiClO_4$, 0.01 M EDOT monomer).[45,46] For each voltammetric cycle, the potential was swept just past the onset for polymer formation (ca. 0.9 V vs Ag/AgCl) and returned to its initial potential. In Figure 2a, the contrast between the clean gold and alkanethiol-stamped gold regions is observed prior to the onset of polymer formation. Figure 2b shows that the first voltammetric cycle produces a sufficient thickness of PEDOT film to bring the alkanethiol-treated and polymer-coated regions of the entire film to approximately the same height, and

(47) Palik, E. D. *Handbook of Optical Constants of Solid*; Academic Press: Orlando, FL, 1985.

(48) Shallcross, R. C.; Chawla, R.; Marikkar F. S.; Tolbert S.; Armstrong, N. R. To be submitted for publication.

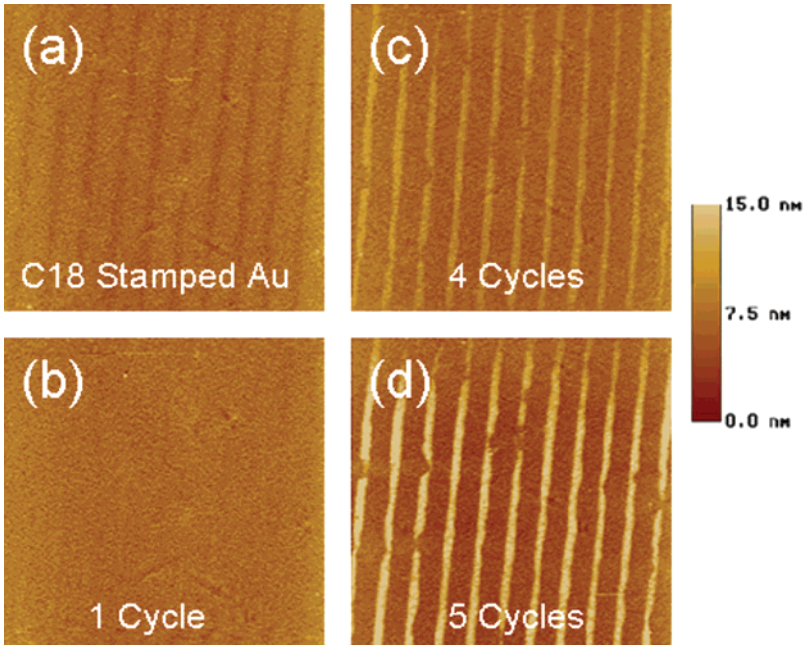

Figure 2. Tapping-mode AFM images (10 μm × 10 μm) of C_{18}-alkanethiol-stamped gold surfaces at various points during voltammetric growth of PEDOT diffraction gratings: (a) AFM image of the freshly stamped Au surface, showing some slight image contrast from the alkanethiol regions (greater stamp pressure led to an alkanethiol pattern width = ca. 400 nm, vs the ca. 250 nm pattern width shown in Figure 1c); (b) the same region after one voltammetric cycle, where the thickness of the PEDOT layer is approximately the same as the alkanethiol layer, resulting in loss of image contrast; (c) the same region after four voltammetric growth cycles; (d) the same region after five voltammetric growth cycles.

this initial image contrast disappears. At this point, ca. 5.5 × 10^{-5} C/cm^2 of PEDOT has been deposited, providing for patterned features of ca. 2 nm thickness. For additional voltammetric cycles, the image contrast improves (Figure 2c) as PEDOT thickness increases, and after five cycles (2.7×10^{-4} C/cm^2), the patterned films are ca. 12 nm in height (Figure 2d). PEDOT growth is initially not uniform, and polymer growth is controlled by nucleation at specific sites under these growth conditions.[49,50] As polymer growth continues, the original nucleation sites coalesce as conductive polymer converges into the bare gold regions. A similar growth mechanism for patterned PANI films was inferred from AFM characterization of films where growth was stopped at grating depths of ca. 5−150 nm.[45,46] From the data in Figures 1 and 2, we infer that gratings are grown with a mainly rectangular grating element shape, owing to the mainly vertical growth of the individual CP strands, away from the electrode surface. For thin polymer films, this rectangular element shape is observed for films that extend well above the thickness of the self-assembled monolayer. Some rounding of the grating element shape is observed for thicker films, which we attribute primarily to difficulties in AFM imaging of such features (i.e., the image shape is a convolution of the actual grating element shape and the shape of the AFM tip).

Evaluation of the DE and CP Grating Development. As shown in Figure 3a, DE was measured for multiple incident angles and for s- or p-polarization of the incident laser in a frontside reflection mode (see also Figure 4f,g). The $m = 1$ line was typically used for these measurements, although the $m = 2$ line was often easily seen. For the data in Figure 3b,c, we used p-polarized 633 nm radiation, at an incident angle of 45°.

Potential step experiments were used to grow both PEDOT gratings (Figure 3b; potential step to +1.0 V vs Ag/AgCl; 10% v/v MeOH, 0.1 M $LiClO_4$ solution, 0.01 M EDOT), and PANI grating (Figure 3c; potential step to +0.7 vs Ag/AgCl; 0.5 M H_2SO_4, 0.05 M aniline). For both systems, the DE increases steadily as grating depth increases, up to DE = ca. 14.6% (for PEDOT; the grating depth that produced the maximum DE was ca. 80 nm) and DE = ca. 26.1% (for PANI; the grating depth that produced the maximum DE was ca. 150 nm). Beyond these grating depths, the DE gradually decreased for patterned PEDOT films, and sharply decreased for the patterned PANI films.

Figure 3d shows the overall DE for an optimized PEDOT grating, normalized to the DE of a grating master such as those used to create the PDMS stamp, using a white light source (Xe-arc lamp). The DE was, at all wavelengths, greater than that for the gold-coated master grating, consistent with the higher refractive contrast with the Au/patterned CP films, and increased in the wavelength region between 500 and 600 nm where the optical properties of gold change significantly. The image of diffracted white light in Figure 1f shows both $m = 1$ and $m = 2$ diffraction orders, indicating high-efficiency CP gratings.

Figure 3b also shows a simulation of DE versus grating depth for grating features with optical constants $n = 1.7$ and $k = 0.14$, on a Au substrate where the superstrate optical constants are $n' = 1.4$ and $k = 0.0$.[45,46] This simulation was normalized to the maximum predicted efficiency and to the grating depth, which provided that maximum efficiency (t/t_{max}). This type of modeling shows that diffraction gratings of this type are expected to increase in efficiency with increasing grating depth, up to a maximum at grating depths of 75−150 nm (depending upon the relative optical properties of the grating and substrate materials), and then decrease until the grating depth is ca. 2× the depth where the first maximum in DE occurred.[45,46]

The details of such simulations are shown in greater detail in Figure 4. Figure 4a−d shows how DE is expected to increase with grating depth for refractive indices of the patterned CP of 1.4, 1.5, 1.6, and 1.7, and a refractive index of the superstrate solution of 1.4. DE is further increased when the grating material has a refractive index of 1.7 and the superstrate solution refractive index is lowered to $n = 1.33$ (Figure 4e). DE is clearly most

(49) Li, F. B.; Albery, W. J. *Electrochim. Acta* **1992**, *37*, 393−401.
(50) Hillman, A. R.; Mallen, E. F. *J. Electroanal. Chem.* **1987**, *220*, 351−367.

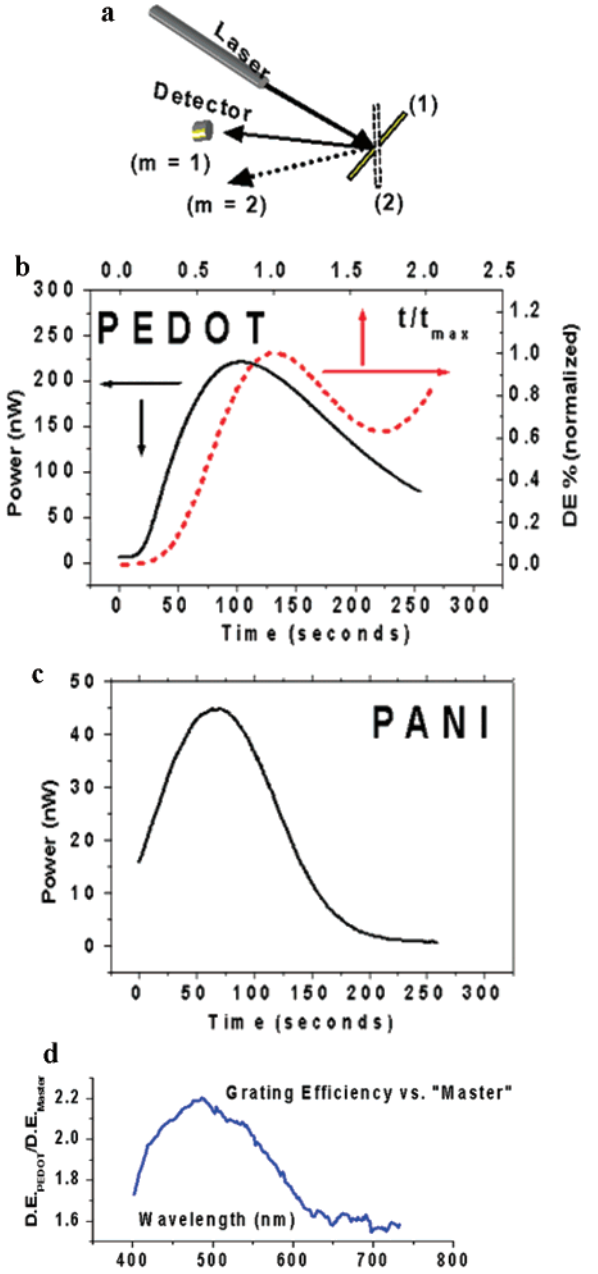

Figure 3. (a) Schematic view of DE measurement showing two different incident angles. (b,c) Output power of $m = 1$ diffraction line for a 5 mW He−Ne laser as a function of electrolysis time after application of a potential step for the growth of (b) PEDOT and (c) PANI gratings, at an angle of incidence of 45°, p-polarization. The dashed red line in panel b also shows the calculated DE vs grating depth for a hypothetical polymer grating on gold, with optical constants $n = 1.7$, $k = 0.14$, superstrate (e.g., solution) and $n = 1.4$, $k = 0$, at 633 nm. This calculated DE is normalized to the maximum predicted (ca. 2%), and the grating depth is normalized to that producing the maximum DE, so as to show the correspondence with the DE vs grating depth data, up to the maximum DE. DE in the real gratings declines after this point due to coalescence of the electrochemically grown polymer features. (d) DE vs wavelength for a typical PEDOT grating under white light illumination, grown to its maximum DE. This data is normalized to the DE versus wavelength data for the grating master used to create the PDMS stamps. The DE of our conductive polymer gratings is highly wavelength dependent and, for PEDOT on Au, reaches 2× the efficiency of the master at ca. 480 nm.

significantly impacted by the refractive index contrast between the polymer forming the grating and the surrounding superstrate solution.[1]

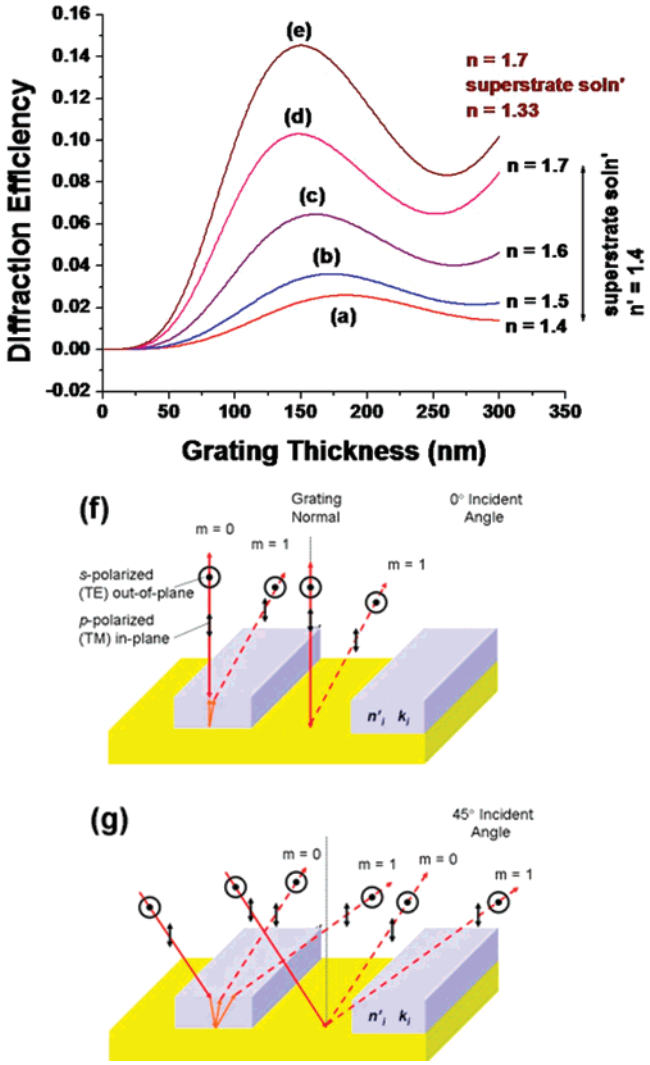

Figure 4. (a−e) Simulated DEs versus grating depth (nm) for various CP gratings: plots a−d represent cases for the systematically increasing refractive index of the CP film, all assuming $k = 0.1$ and an $n = 1.4$ for the superstrate solution; plot e represents the added increase in DE expected when the refractive index of the superstrate solution decreases to $n = 1.33$, i.e., the refractive index contrast increases. Panels f and g are schematic representations of the various optical geometries utilized in characterization of DE during and after the growth of the patterned CP films: diffraction ($m = 1$) at incident angles of 0° (f) and 45° (g). Both s- and p-polarization were used in the incident beams.

Estimation of the Optimum Sensitive Region via Modeling and Simulation. For CP films, changes in DE are anticipated as a result of changes in both the real (n) and imaginary (k) components of refractive index ($n^* = n + ik$), and the grating thickness:[1,51]

$$\mathrm{DE}_{(\lambda)} = \mathrm{e}^{-2.303OD(\lambda)/\cos\theta}\left[\frac{T}{\lambda \cos\theta}\right][\Delta k_{(\lambda)}{}^2 + \Delta n_{(\lambda)}{}^2] \quad (1)$$

Several simulated examples (using Grating Solver) are shown in Figure 5, where we consider s-polarized 633 nm radiation, a 45° incidence angle, and a rectangular grating element shape to calculate the grating sensitivity response, as shown below.

It is of interest to predict at which grating thicknesses the sensitivity toward chemical changes to the CP film would be maximized, which of course will be strongly dependent upon the

(51) Fayer, M. D. *Annu. Rev. Phys. Chem.* **1982**, *33*, 63−87.

optical properties of the CP, the wavelength of excitation, the shape of the grating element, and the substrate and superstrate optical properties. We first define the absolute sensitivity of a chemically responsive diffraction grating (AS_n) as the first derivative of grating efficiency with respect to changes in n or k (equivalent relationships would be written for both parameters):

$$AS_n = \frac{\partial \eta}{\partial n} \approx \frac{\Delta \eta}{\Delta n} \text{ for } k = k_0 \quad (2)$$

AS_n (AS_k) is a dimensionless number, such that, for a given Δn (Δk), the resulting absolute change in DE can be calculated as

$$\Delta \eta = AS_n \cdot \Delta n \quad (3)$$

Most measurements will record the change in relative intensity of the diffracted light upon change in the optical constants of the grating. Therefore, a relative sensitivity (RS_n or RS_k) is defined in terms of the change in the relative intensity of the diffracted light versus the change in n or k for the grating:

$$RS_n = \frac{AS_n}{\eta} \quad (4)$$

RS_n (RS_k) is also a dimensionless number, and, for a given Δn (Δk), the relative percent change in efficiency can be calculated:

$$\frac{\Delta \eta}{\eta} = RS_n \cdot \Delta n \cdot 100\% \quad (5)$$

Sensitivity products (PS_n) can then be defined as the product of AS_n and RS_n (or AS_k and RS_k):

$$PS_n = AS_n \cdot RS_n = \left(\frac{\partial \eta}{\partial n}\right)^2 \cdot \frac{1}{\eta} \cdot \sin(AS_n) \approx \left(\frac{\Delta \eta}{\Delta n}\right)^2 \cdot \frac{1}{\eta} \cdot \sin(AS_n) \quad (6)$$

As expected, high values of AS_n are not useful in cases where DE is high (representing a high background signal), and high values of RS_n are not useful when AS_n is small (and therefore not measurable). The product of AS_n and RS_n can therefore be used to predict a grating depth that maximizes PS_n. Simultaneous changes in n and k can also be studied by considering the combined sensitivity to both these parameters.

Figure 5 summarizes the sensitivity products (PS_n and PS_k) for weakly absorbing ($k = 0.1$), moderately absorbing ($k = 0.5$), and strongly absorbing ($k = 1.0$) gratings. Qualitatively similar results are obtained whether s- or p-polarization of the incident beam is assumed. The sensitivity product versus grating depth plots are best defined and easiest to understand for weakly absorbing CP films, $k = 0.1$. PS_n shows the largest changes versus grating depth, and in all cases, PS_n maximizes before PS_k. This is supported by the relative and absolute sensitivity calculations in the Supporting Information (Figure S1), which shows sensitivity minima at thicknesses where the grating achieves its maximum efficiency. As might be expected for any technique that relies upon changes in reflectivity as a function of CP film thickness, these materials are most responsive to chemical or electrochemical changes when they are quite thin. Further optimization is possible by using longer wavelengths because of the strong Au reflectivity, and through consideration of the anisotropic properties of the polymer film.[47] These results were of course obtained by assuming rectangular grating element shapes, and it is clear that different grating shapes would provide different sensitivities and different sensitivity products. However, since these electrochemically grown gratings had a mainly rectangular shape, we confined our modeling studies to those shapes as well.

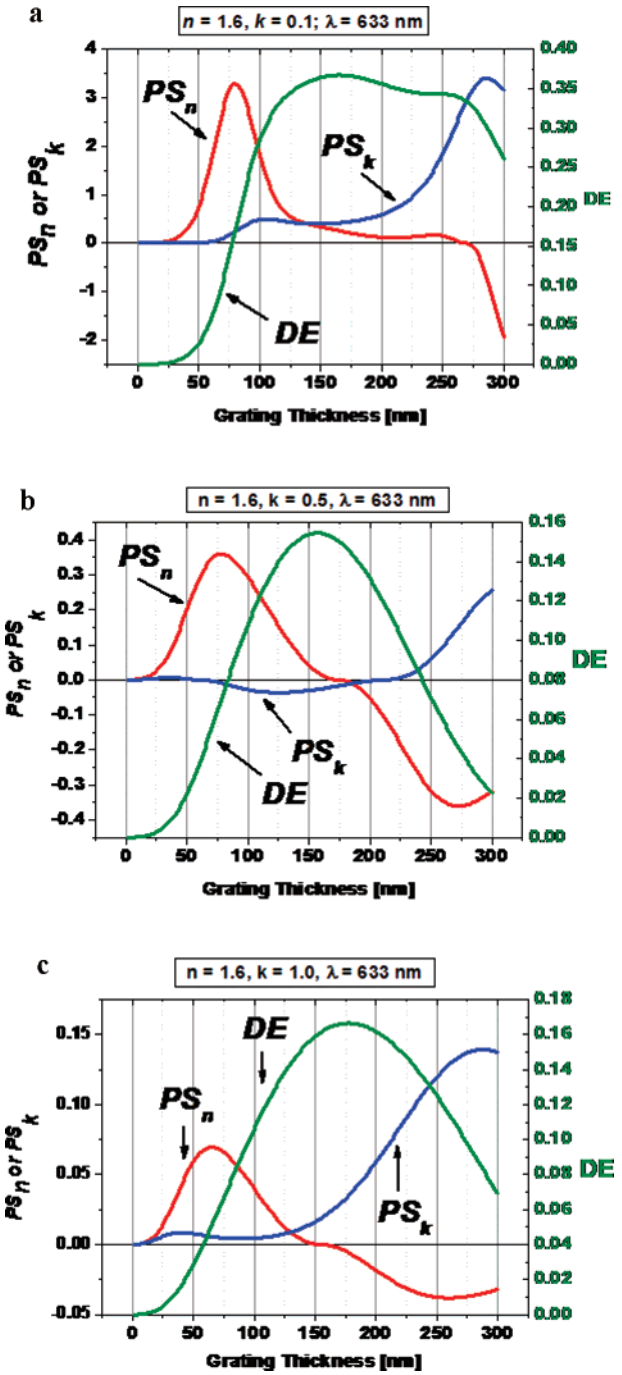

Figure 5. Sensitivity products (PS_n) and DEs versus grating depth calculated for three different gratings on Au: (a) $k = 0.1$, (b) $k = 0.5$, and (c) $k = 1.0$. The refractive index (n) for the patterned CP film was assumed to be 1.6 at 633 nm for s-polarized radiation, incident at 45°. The sensitivity product in terms of refractive index, PS_n, is clearly larger at all grating depths than the sensitivity product in terms of k, PS_k, and its maxima occur at shallower grating depths.

Changes in DE Induced by pH Changes and Applied Potential. Using the findings of these simulations, we characterized the pH dependence of the DE of PANI gratings with potentiostatically grown gratings, the greatest sensitivities were obtained with grating depths yielding 25−50% of the maximum DE. The Au electrode substrate was held at (*i*) open circuit or (*ii*) +0.4 V, as various buffer solutions were introduced into the cell, without change of grating position. Both s- and p-polarization of the incident He−Ne laser were used, with incident angles of both 0° and 45°. Results using p-polarization of the incident beam, which showed the greatest pH sensitivity, are shown.

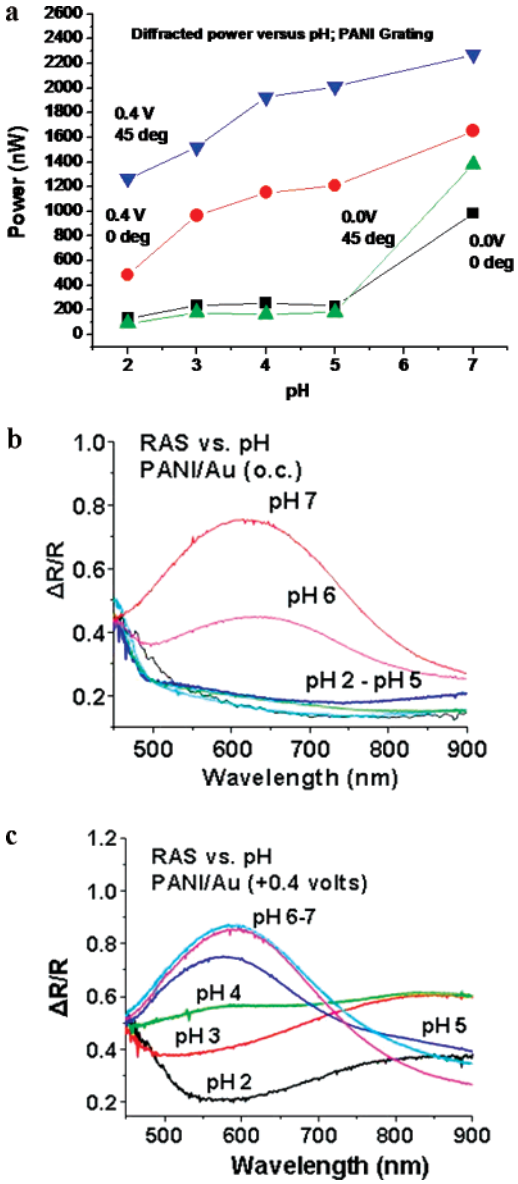

Figure 6. (a) Power of diffracted He−Ne laser ($m = 1$) beam versus pH for both 0° and 45° incident beams, where ca. 50 nm depth PANI/Au grating electrodes were either held at +0.4 V, or were allowed to sit at open-circuit (potentiometric mode); (b,c) reflection/absorption spectra for comparable thickness PANI films as a function of pH at open-circuit (b) and +0.4 V (c).

At open circuit there is only a small dependence of DE versus pH, regardless of polarization or incident angle, until pH ≥ 5 is reached, whereupon there is an abrupt rise in DE. For PANI gratings held at +0.4 V, where the PANI film is predominantly in the emeraldine salt (ES) form, in equilibrium with the emeraldine base (EB) form,[2,3,10,15,21,52,53] there is a monotonic rise in DE with pH: DE increases by 2 to 3 times as pH is increased from 2 to 7, and in general, there is a higher DE for 45° versus 0° incidence of the He−Ne laser. A higher ΔDE was obtained for p-polarized radiation over s-polarization, which can arise as a result of the optical anisotropy of the grating itself with the possibility of some contribution from the anisotropy in the optical properties of the patterned PANI film.[54,55]

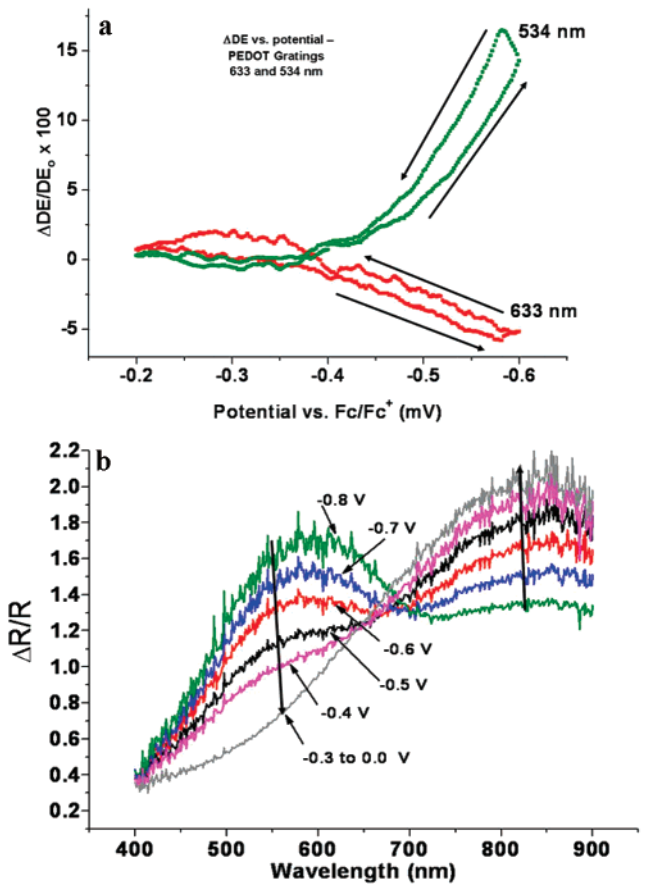

Figure 7. (a) Change in DE vs potential (vs Fc/Fc^+) for a ca. 50 nm depth PEDOT grating (grown potentiostatically in MeCN/$LiClO_4$), using 534 and 633 nm lasers with p-polarization at an incident angle of 45°. (b) Reflection/absorption spectra vs applied potential for a similar thickness non-patterned PEDOT film on Au.

The reflection/absorption spectra for non-patterned PANI films of comparable thickness were also obtained as a function of pH, indicating relatively small differences in the imaginary component of the refractive index, whether the PANI films were held at 0.0 V (data not shown),[46] open circuit, or at +0.4 V (Figure 6b,c, respectively). The changes in DE vs pH for these PANI films must arise primarily from changes in n as the pH increases and the ES ↔ EB equilibrium shifts toward the EB form of the polymer. Kramers−Kronig transformations were applied to these reflectivity data to obtain estimates of n and k (Supporting Information, Figure S2).[1,2] A maximum Δn of ca. 0.4 and a Δk of ca. 0.1 occur between pH = 2 and pH = 7 for PANI thin films at 633 nm (Figure S2a), agreeing with the above characterization of optical changes. Similar changes in reflectivity were seen for both thicker and thinner PANI films, but the relative changes in DE were largest for gratings with a depth of ca. 50 nm.

The optical properties of patterned conductive polymers, such as PEDOT, are also easily modulated by changes in applied potential.[5,7,19,55−58] These phenomena have been associated with oxidation-induced film swelling and anion/solvent exchange during the transformation from a neutral to a positively charged film. Figure 7 shows the changes in DE versus applied potential

(52) Huang, W. S.; Humphrey, B. D.; Macdiarmid, A. G. *J. Chem. Soc., Faraday Trans. 1* **1986**, *82*, 2385−2400.
(53) Macdiarmid, A. G.; Chiang, J. C.; Richter, A. F.; Epstein, A. J. *Synth. Met.* **1987**, *18*, 285−290.
(54) Ou, R. Q.; Gerhardt, R. A.; Samuels, R. J. *J. Polym. Sci., Part B: Polym. Phys.* **2003**, *41*, 823−841.
(55) Liu, J. Y.; Tian, S. J.; Tiefenauer, L.; Nielsen, P. E.; Knoll, W. *Anal. Chem.* **2005**, *77*, 2756−2761.
(56) Pettersson, L. A. A.; Johansson, T.; Carlsson, F.; Arwin, H.; Inganas, O. *Synth. Met.* **1999**, *101*, 198−199.
(57) Pettersson, L. A. A.; Ghosh, S.; Inganas, O. *Org. Electron.* **2002**, *3*, 143−148.
(58) Pile, D. L.; Zhang, Y.; Hillier, A. C. *Langmuir* **2006**, *22*, 5925−5931.

for a patterned PEDOT film, after its initial growth in acetonitrile ($LiClO_4$ electrolyte), using both 534 and 633 nm laser sources (p-polarization, 45° incident angle). Similar changes were noted for PEDOT films grown in MeOH/H_2O, but were larger and better defined for PEDOT polymers grown in the nonaqueous solvent. The DE vs potential changes shown in Figure 7a were reproduced exactly as shown as potential was cycled several times from −0.2 to −0.8 V (vs Fc/Fc+); however, for clarity, only one cycle is shown. The RAS data for a comparable thickness uniform PEDOT film on Au is shown in Figure 7b, showing the changes in absorptivity that occur during cycling of the potential between 0.0 and −0.8 V. These are potentials known to cycle the PEDOT film between its neutral and oxidized (doped) forms (Figure S3),[46,59] and cyclic voltammetric experiments indicate a small Faradaic current flowing in these patterned films during the potential sweep to positive potentials, indicating oxidation of ca. 75% of the EDOT monomer units in the PEDOT chains at −0.2 V. It is interesting to note that the DE of the PEDOT grating markedly increases at 534 nm as the electrode potential is cycled from the partially oxidized state of PEDOT to its neutral state, while the DE at 633 nm decreases during these same potential changes. These two laser wavelengths fall on the blue and red side, respectively, of the main absorbance band of the fully reduced PEDOT layer at ca. 570 nm.[60] Both Δk (ca. 0.1) and Δn (ca. 0.2) may contribute to the modulation of the DE at 534 nm. According to the Kramers−Kronig relation (Figure S2b) a higher DE is predicted at 633 nm (Δk = ca. 0.3, Δn = ca. 0.6), although, in contrast, a negative response is observed. Examples have been shown where the DE modulations at electroactive polymers cannot always be explained by considering the optical data alone[1] (e.g., occasions where the electrolyte solution has a refractive index between that of the doped and dedoped states of the CP film,[8] or where there are changes in the thickness of the polymer.[1,38,51]

(59) Kumar, A.; Welsh, D. M.; Morvant, M. C.; Piroux, F.; Abboud, K. A.; Reynolds, J. R. *Chem. Mater.* **1998**, *10*, 896−902.

(60) Hwang, J.; Tanner, D. B.; Schwendeman, I.; Reynolds, J. R. *Phys. Rev. B* **2003**, *67*, 115205-1−115205-10.

Conclusions and Future Directions

CP periodic arrays can be routinely constructed at the submicron length scale with the combination of microcontact printing and electropolymerization. Efficient DE responses can be obtained in the visible range and can be measured using a simple photodiode. The initial modulation of the DE in the presence of an analytical stimulus (pH, potential) at these surfaces suggest that additional sensing capabilities such as biomolecule binding can also be incorporated. These electroactive periodic arrays may also undergo DE changes upon chemical reduction[1,2] or electrocatalysis[3] in the presence of redox species in solution. Simulations of these processes with realistic optical constants may serve to simplify the actual experimental process during sensor optimization. We have also recently observed the formation of even more efficient transmission grating elements using semiconductor nanoparticles as the "ink" in the microcontact printing step.[48] In these cases, the refractive index contrast between the grating element and the superstrate medium is even greater than that for the CP films discussed here, and grating patterns up to 2400 lines/mm are easily achievable. Future sensing platforms seek to combine these particles with a CP platform, using the sensitivity criteria discussed here.

Acknowledgment. This work was supported by a grant from the National Science Foundation, CHE 0517963, the NSF Center for Materials and Devices for Information Technology − DMR-0120967 Chemical Sciences, and the Geosciences and Biosciences Division, Office of Basic Energy Research, U.S. Department of Energy, DE-FG03-02ER15378. N.R.A. would like to gratefully acknowledge support by the Alexander von Humboldt Stiftung for a Senior Research Prize while at the Institut für Angewandte Photophysik, T.U.-Dresden.

Supporting Information Available: Additional grating efficiency simulations, the Kramers−Kronig analyses for both PANI and PEDOT films, and spectroelectrochemical characterization of PEDOT films. This information is available free of charge via the Internet at http://pubs.acs.org.

LA701369H